Data Repository Item

Seismic imaging of subduction zone metamorphism

S. Rondenay, G. A. Abers & P.E. van Keken

1- ROBUSTNESS AND RESOLUTION OF THE SEISMIC IMAGES

The seismic images presented in the paper are produced by multichannel inversion of scattered teleseismic P waves incident on dense arrays of seismographs (see, e.g., Bostock et al., 2001; Rondenay et al., 2005). This approach is similar to the receiver function method, which has provided some of the earliest samples of slab structure (Langston, 1979), but extends it in several ways to provide images with higher spatial resolution. The problem is posed for forward- and back-scattered wavefields generated at discontinuities in a 2D isotropic medium, with the backprojection operator cast as a generalized Radon transform (GRT). The approach (hereafter referred to as 2D GRT inversion) allows for the treatment of incident plane waves from arbitrary backazimuths, and recovers estimates of material property perturbations (e.g., S velocity) about a smoothly varying reference model.

The 2D GRT inversion relies on certain simplifying assumptions and a comprehensive data sampling to insure the robustness of the images and a high resolution of target structure. Its applicability and resolving power has been extensively studied for general applications (Shragge et al., 2001; Rondenay et al., 2005), but some aspects its robustness and resolving power can only be assessed based on the specific attributes of a given study

area. These attributes include the sampling geometry, the geometry of the imaging target, and the seismic illumination. An assessment of these attributes has already been conducted for the Cascadia image (see, e.g., Rondenay et al., 2001) and shows that the structure there is well resolved, but it has not yet been done for Alaska. Here, we therefore address the applicability and resolution of 2D GRT inversion in southern Alaska.

1.1- Target structure and 2-D geometry

A central assumption to the 2-D GRT inversion is that scattering occurs at 2-D (i.e., line) scatterers – a simplification of the problem that stems from the limited availability of broadband seismic sensors, meaning that dense linear arrays are more easily realizable that 2-D regional arrays. It is therefore important to determine the 2-D regional strike and test the validity of the 2-D assumption to ensure that the main features observed in the final image are not related to mismapping of, or artifacts due to, out-of-plane structure.

We first determine the strike of the imaging target – in this case the subducted slab. This is achieved by mapping the slab depth contours in the study area based on the Wadati-Benioff seismicity map of Ratchkovski and Hansen (2002). These contours are shown in map view in Figure DR1, and from this we determine an average strike of N240E. The seismic profiles are therefore constructed along a line with azimuth N150E, as in the preliminary receiver function study of Ferris et al. (2003).

Second, we assess the validity of the 2-D assumption. This geometrical requirement is validated by insuring that two-dimensionality is preserved within a region defined by the maximum lateral offset (perpendicular to the projection line) from where detectable scattered signal is produced. It can be shown that for a target at 150 km depth, the minimum lateral extent on either sides of the station array is of the order of 75 km (Rondenay et al., 2005). Based on the slab contours shown in Figure 1 we see that the slab does extend laterally over such distance relative to the middle of the array. An exception to this rule might be encountered at the northwestern end of the line, which is close to the end of the seismically-defines slab. However, this would affect the image generated by events illuminating the slab obliquely from the NNE, but as shown in the next section (see Figure DR2) very few events from that quadrant are used. We also observe that the southernmost stations are near a bend in the seismically-inferred slab, which could represent a departure from the 2-D assumption. However, since the low-velocity layer is at 50km depth is this part of the profile, the minimum required offset on this structure here is reduce to only 25 km – a requirement that is met by the slab. Furthermore, images were produced using only subsets of events illuminating the region from various backazimuthal bins (to be presented in a companion paper) and all show a consistent signal (thickness and velocity perturbation) for the low-velocity layer between 50-120 km depth. The slab can therefore be considered as a 2-D structure beneath our study area.

1.2- Comprehensive (two-sided) teleseismic illumination

Another important factor affecting the robustness of the image is the illumination of the target structure by incident teleseismic waves. Incomplete illumination inhibits the focusing of the final image. Of particular importance, in the case of a target structure such as a dipping subduction slab, is the requirement that the slab be illuminated with both updip and downdip incidence (Rondenay et al., 2001). This insures that slab-parallel features (e.g., subduction décollement, oceanic Moho) are detected by both forward and back scattered waves, respectively. In the case of Alaska, the study area must therefore be illuminated from both the SSE hemisphere (backazimuths ranging between N60E-N240E) and from the NNW hemisphere (backazimuths ranging between N240E and N60E), a requirement that is satisfied by the distribution of events used in the analysis (see Figure DR2).

1.3- Dip resolution

The dip resolution is controlled by the dip angle of the spatial gradient of total travel time function ∇T (i.e., scattered wave – incident wave), a vector quantity representing the sensitivity of total travel time to scatterer location (see Bostock et al., 2001; Rondenay et al., 2005). As shown in Rondenay et al. (2005), the dip resolution at any point of the model can be determined by plotting the range of vectors ∇T that is achieved by combining all the event-station waveform pairs for that given point. The spherical representation of vectors ∇T at a scattering point is known as an Ewald sphere, and its

visual analysis allows a rapid assessment of the dip resolution at that point. In Figure DR3a, we show an Ewald sphere near the center of the profile (horiz. dist. = 100km, depth = 80 km in Fig. 2a,c of the paper), where the data set achieves a symmetric and complete dip resolution, ranging between [-90°, 90°].

As the range of dip resolution decreases with depth and becomes asymmetric to the sides of the profile, we must verify that the termination of the low-velocity layer beneath Alaska is not an artifact due to decreased dip resolution. Figure DR3b shows the Ewald sphere near the termination point (horiz. dist. = 150 km, depth = 120 km in Fig. 2a,c of the paper), where the data set achieves a dip resolution ranging between [-63°, 88°]. This means that structure dipping to the NNW at an angle >60° relative to the surface is not well resolved. In this region of the profile, Wadati-Benioff seismicity (Ratchkovski and Hansen, 2002) indicates that the slab extends to depths ≥150 km at an average dip angle ≤ 60° (although some clusters of events seem to plunge with greater dips), suggesting that slab parallel structure should be robustly resolvable down to at least 150km depth. Moreover, if the low-velocity layer extended to greater depth with a dip exceeding that of the maximum resolvable dip, the layer would still be observed below 120km depth, but it would be more diffuse and it would show an erroneous dip – a common artifact in seismic migration (see, e.g., Yilmaz, 2001). Such continuation of the low-velocity layer is not observed here below 120 km depth. Based on these arguments, we can conclude that the termination of the low-velocity layer near ~120 km depth in the NNW portion of the seismic profile is a robust feature.

1.4- Volume resolution and tapering of the low-velocity layer

Volume resolution depends on the wavelength of the scattered signal considered in the analysis. The best resolution (i.e., smallest resolvable structure) is determined by the smallest wavelength (λ), which for P-to-S scattered waves is of the order of 12-15 km in the crust and upper mantle, for a high cut-off frequency of 0.3 Hz as that used here in both Cascadia and Alaska. Higher frequencies are filtered to remove the effects of scattering from topography at the free-surface (see Rondenay et al., 2005). The average resolution for forward scattered waves is $\sim\lambda/2$=6-8 km, whereas that for back-scattered waves is $\sim\lambda/4$=3-4 km (see Bostock, 1999; Rychert et al., 2005, 2007). The best resolution is therefore afforded by back-scattered waves (i.e., free-surface multiples) and is ~3-4 km. This means that scatterers separated by at least 3-4 km can be distinctly identified and well characterized. This quantity also corresponds to the minimum thickness resolvable for discreet homogeneous layers.

In our image of Alaska (Figure 2a,c in the paper), a tapering of the dipping low-velocity layer is observed for waves illuminating the study area from all available azimuths, and therefore appears to be a robust feature across the entire imaging volume. However, previous analyses showed that the layer thickness was constant at ~20 km from 50-120 km depth (Ferris et al., 2003). Here, we show that previous and new results may be reconciled by taking into account the increase in resolution resulting from the inclusion of back-scattered waves in the imaging technique used in this paper. We define the sensitivity of seismic waves to velocity gradients as their ability to detect such gradients

as discontinuities, and can show that this sensitivity decreases with increased resolution. Following the definition of volume resolution presented above, a clear discontinuity will be observed if the gradient occurs over a thickness smaller than $\lambda/2$ for the transmission case, and $\lambda/4$ for the reflection case. Figure DR4 shows a simple model that can explain the observed discrepancy between an image obtained with only forward-scattered waves and one that includes back-scattered ones. In this case, the forward transmitted waves see both the sharp velocity jump and the overlying velocity gradient as discontinuities. These are close enough in time to produce one single peak. Conversely, the back-scattered waves only detect the sharp velocity jump. This finding supports a model where the low-velocity layer comprises two sub-layers: a top layer containing a velocity gradient occurring over 10 km, that is likely indicative of progressive dehydration with depth; and a lower layer displaying more uniform low-velocity.

1.5- Aliasing

Aliasing occurs when the scattered signal and/or the weighting function in the imaging operator are under-sampled, resulting in artifacts that degrade the robustness of the images. Rondenay et al. (2005) show that aliasing may affect the image between the surface and a depth corresponding to twice the station spacing. In the case of Alaska, since the station spacing is ~10 km, structure imaged at depths >20 km should therefore not suffer from aliasing – which applies to the dipping low-velocity layer.

2- THERMAL MODELS

The model for Alaska (Figure DR5A) is identical to the reference model shown in Abers et al. (2006). The lithospheric age at the trench is 38 Ma and the plate subducts with a speed of 55 mm/yr. The model geometry matches the location of the seismically imaged low velocity zone. A small component of shear heating corresponding to a stress of 10MPa is applied along the slab-wedge interface, to a depth of 80 km. The subducted slab is kinematically prescribed. It dynamically drives flow in the wedge, which is modeled using a dry olivine rheology. To match the observed low attenuation corner in the tip of the wedge we reduce the effective coupling between slab and wedge to 80 km depth. The governing equations are solved using a high-resolution finite element model with local grid resolution in the boundary layers of less than 1 km.

The thermal model for Cascadia (Figure DR5B) is similar to that of Alaska, but with a geometry modified to match the seismically observed location of crust and serpentinized corner in the mantle wedge. The incoming plate age is 7.5 Ma and subducts at 35 mm/yr. No shear heating is assumed along the seismogenic zone.

References cited

Abers, G.A., van Keken, P.E., Kneller, E.A., Ferris, A., and Stachnik, J.C., 2006, The thermal structure of subduction zones contrained by seismic imaging: implications for slab dehydration and wedge flow: Earth Planet. Sci. Lett., 241, 387-397.

Bostock, M. G., 1999, Seismic imaging of lithospheric discontinuities and continental evolution: Lithos, v. 48, p. 1–16.

Bostock, M. G., Rondenay, S., and Shragge, J., 2001, Multiparameter two-dimensional inversion of scattered teleseismic body waves, 1, Theory for oblique incidence: Journal of Geophysical Research, v. 106, p. 30,771–30,782.

Ferris, A., Abers, G. A., Christensen, D. H., and Veenstra, E., 2003, High resolution image of the subducted Pacific (?) plate beneath central Alaska, 50–150 km depth: Earth and Planetary Science Letters, v. 214, p. 575–588.

Langston, C. A., 1979, Structure under Mount Rainier, Washington, inferred from teleseismic body waves: Journal of Geophysical Research, v. 84, p. 4749–4762.

Ratchkovski, N., and Hansen, R., 2002, New evidence for segmentation of the Alaska subduction zone: Bulletin of the Seismological Society of America, v. 92, p. 1754–1765.

Rondenay, S., Bostock, M., and Fischer, K., 2005, Multichannel inversion of scattered teleseismic body waves: Practical considerations and applicability, in Levander, A., and Nolet, G., eds, Seismic Earth: Array analysis of broadband seismograms: Washington, DC, American Geophysical Union, Geophysical Monograph, v. 157, p. 187–204.

Rondenay, S., Bostock, M. G., and Shragge, J., 2001, Multiparameter two-dimensional inversion of scattered teleseismic body waves, 3, Application to the Cascadia 1993 data set: Journal of Geophysical Research, v. 106, p. 30,795–30,808.

Rychert, C. A., Fischer, K. M., and Rondenay, S., 2005, A sharp lithosphere-asthenosphere boundary imaged beneath eastern North America: Nature, v. 436, p. 542–545.

Rychert, C. A., Rondenay, S., and Fischer, K. M., 2007, P-to-S and S-to-P imaging of a

sharp lithosphere-asthenosphere boundary beneath eastern North America: Journal of Geophysical Research, (in press).

Shragge, J., Bostock, M., and Rondenay, S., 2001, Multiparameter two-dimensional inversion of scattered teleseismic body waves, 2, Numerical examples: Journal of Geophysical Research, v. 106, p. 30,783–30,794.

Yilmaz, O., 2001, Seismic data analysis: Tulsa, Oklahoma, Society of Exploration Geophysicists, 2027p.

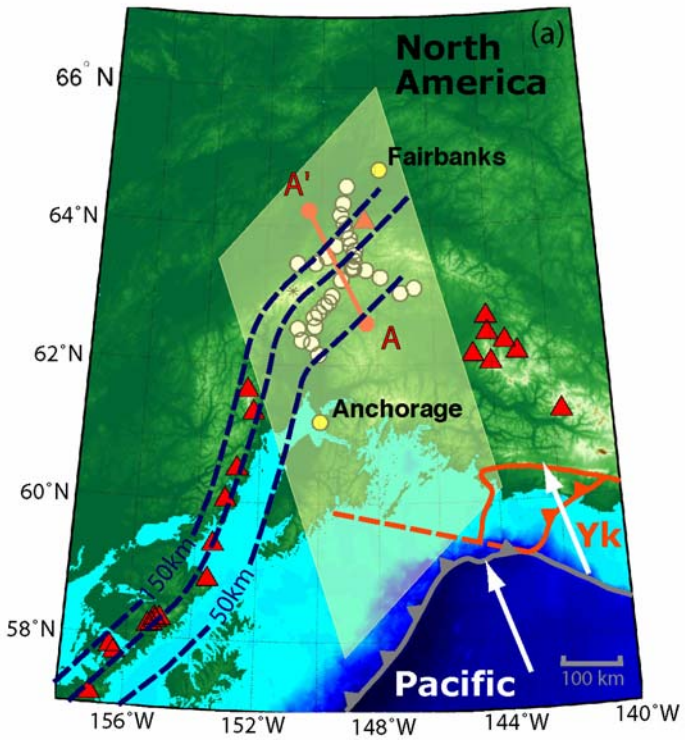

Figure DR1. Map of the study area showing the depth countours of the subducted slab based on Wadati-Benioff seismicity (Ratchkovski and Hansen, 2002). Yellow shaded area denotes of the Denali segment of the subducted slab. See caption of Figure 1 (paper) for the description of other symbols and lines.

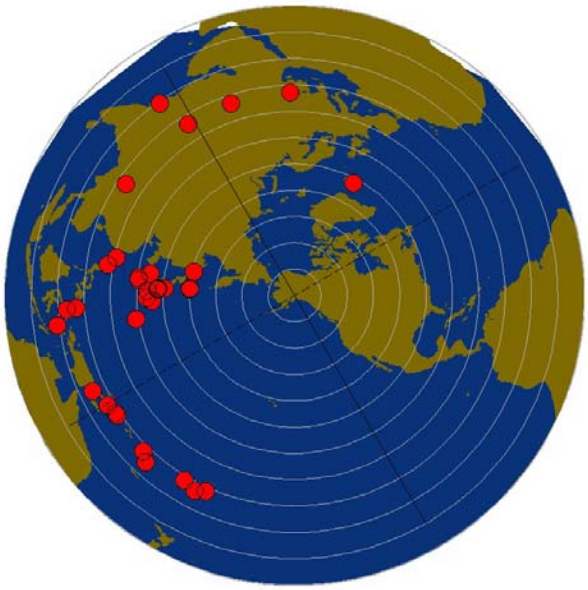

Figure DR2. Distribution of teleseismic earthquakes used to produce the seismic image of the central Alaska subduction zone (Figure 2a,c of paper). Earthquakes are denoted by red circles, and represented in polar projection centered on the study area. Cross lines represent the projection of the seismic profile (solid) and the estimated 2-D strike of the slab (dashed). Concentric white circles denote the epicentral distance from the center of the array, by increments of 10°.

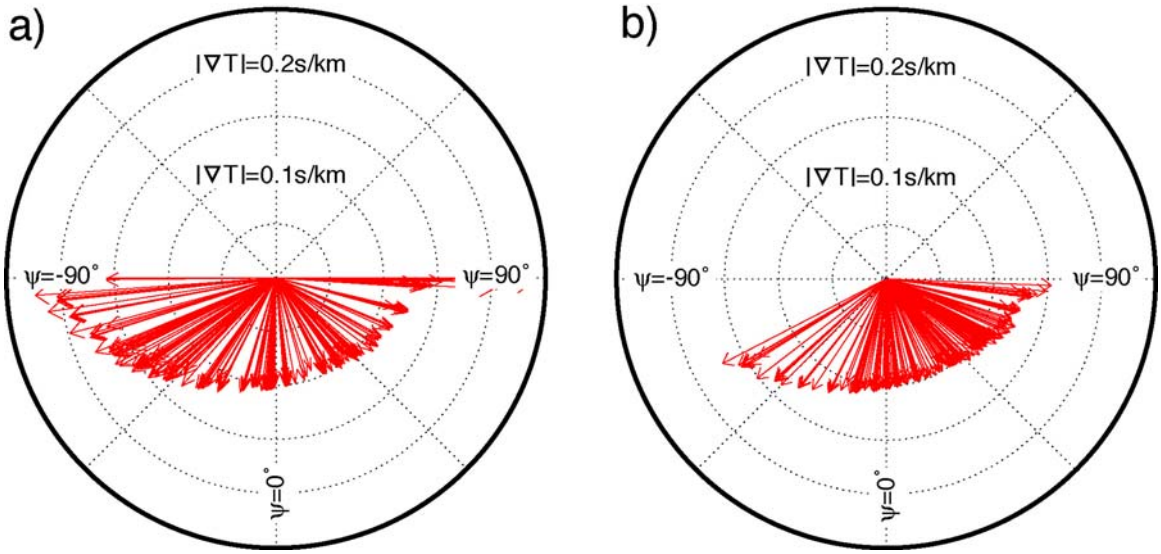

Figure DR3. Ewald sphere analysis for (a) a scatterer located near the center of the seismic image (horiz. dist. = 100km, depth = 80 km), and (b) a scatterer located near the termination point of the low-velocity layer (horiz. dist. = 150km, depth = 120 km), Red vectors represent the spatial gradient of total travel time function ∇T. Dotted lines show the magnitude of these vector |∇T|, and their dip angle ψ. Surfaces perpendicular to these vectors can be resolved in the seismic image.

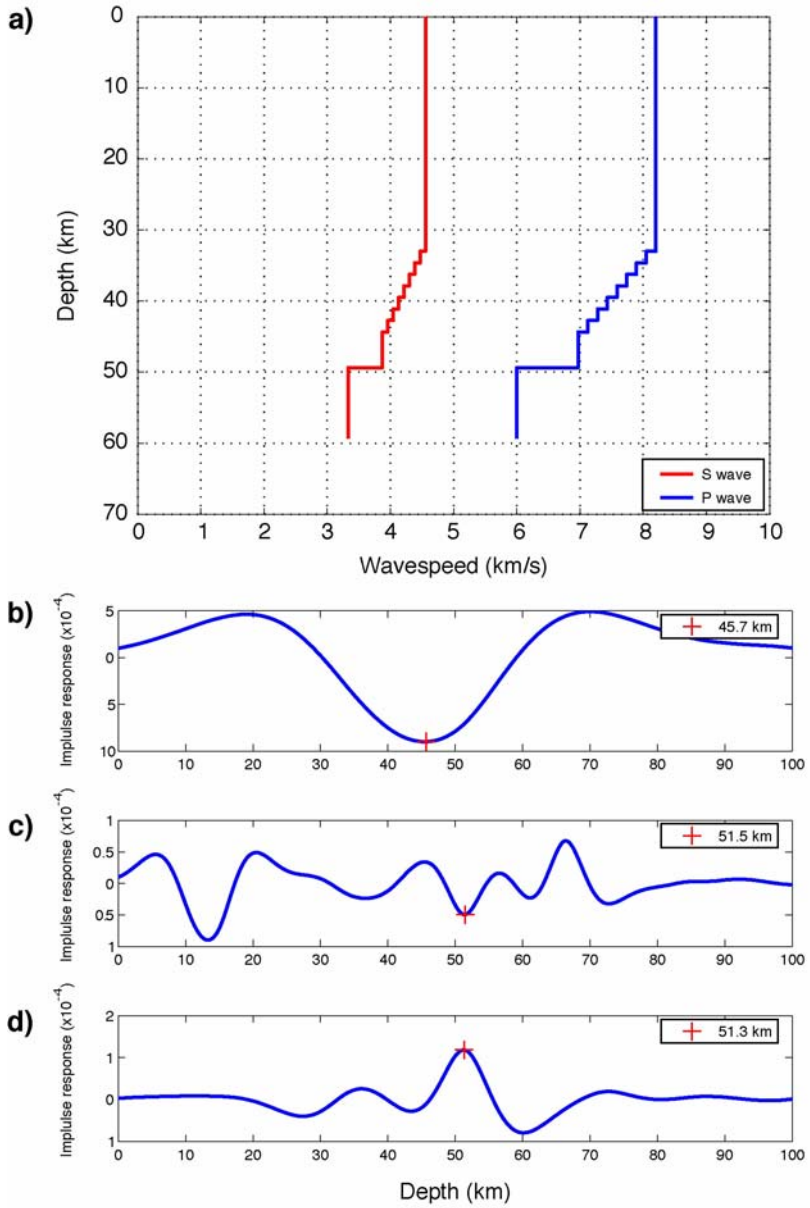

Figure DR4. Synthetic model explaining the discrepancy in resolution between forward and back scattered waves. (a) 1-D velocity model containing a negative velocity gradient at 33km depth, followed by a sudden velocity drop at 50km depth. Synthetic receiver functions are calculated with a reflectivity code, for a wave incident from the left with horizontal slowness p=0.03s/km and a dominant period of 4 s. The receiver functions are 1-D depth migrated to phasing depth corresponding to phases (b) forward scattering Ps, (c) back scattering Pps, and (d) back scattering Pss. The main phases associated with the velocity structure in (a) are indicated by a red cross. The forward-scattered mode (b) is sensitive to both the velocity gradient and the velocity drop, whereas the back-scattered modes (c-d) are mainly sensitive to the velocity drop. This different in sensitivity results in a depth discrepancy $>$5km, similar to that observed in the migrated images.

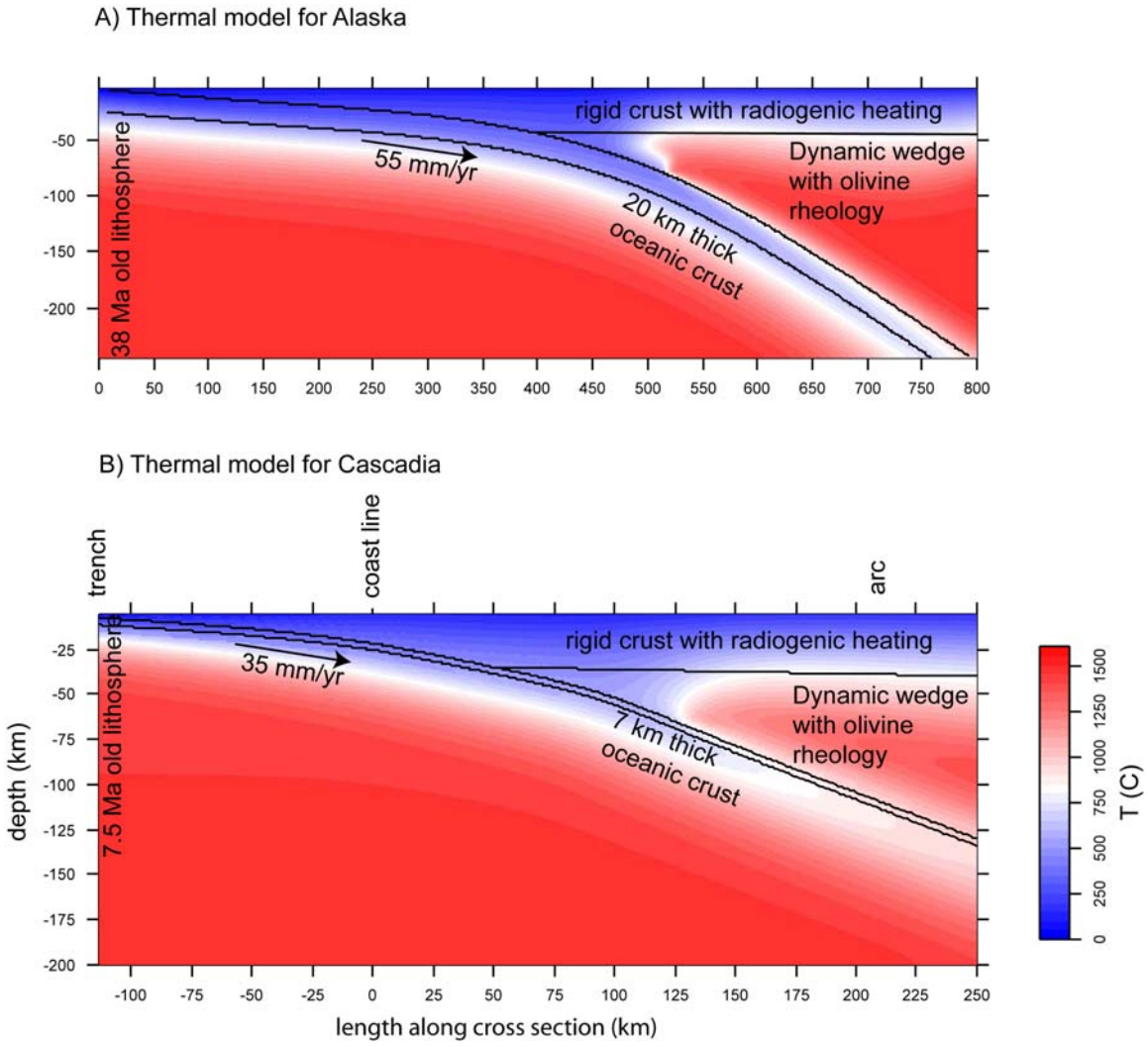

Figure DR5. Thermal models for the A) Alaska and B) Cascadia transect.